POAC'13
Espoo, Finland

Proceedings of the 22nd International Conference on
Port and Ocean Engineering under Arctic Conditions
June 9-13, 2013
Espoo, Finland

DISTRIBUTION OF ICE VOLUME CONTENT IN SEA ICE RIDGES

Victor V. Kharitonov

Arctic and Antarctic Research Institute, St. Petersburg, Russia

ABSTRACT

Thermal drill penetration rate records during hot water and electric drilling of ice ridges provide information about their internal structure. Drill penetration rate is inversely proportional to the volume content of solid phase of ice. The dependence of the value reciprocal of the rate of drilling versus depth is the dependence of volume content of the solid phase of ice versus depth, or, in other words, the distribution of solid phase along the borehole. Averaging these distributions for all boreholes, one can obtain average statistical distribution of the volume of the solid phase of ice with depth both for a single ice ridge, and for all ice ridges located within the area investigated. The paper addresses the results of model analysis of distribution of volume content of ice solid phase with depth for an ideal ice ridge. The examples of the distribution for real ice ridges are provided. By the form of these distributions, location of the boundaries of the consolidated layer of ice ridge and its average thickness can be estimated. Behavior of the dependence of the volume content of ice solid phase with depth in unconsolidated areas of the sail and keel points to the distribution of the porosity of the ice ridge, the presence of particular features in its structure.

INTRODUCTION

An ice ridge is a hill-shaped chaotic conglomeration of broken ice, formed as a result of compression, being afloat and partly frozen. Internal structure of ice ridges is determined by randomly oriented fragments of ice, in the result of freezing of which the backbone of an ice ridge formation with complicated spatial structure is formed. The validity of calculations of loads of ice ridge on offshore structures depends on how precisely its internal structure was determined. The gaps between the ice blocks are filled with air, snow, water or shuga. In addition, ice blocks contain pores filled with brine and air bubbles. In this paper the volume content of ice in an ice ridge refers to the relative volume occupied by solid-phase ice in one cubic meter of the ice ridge. Obviously, the ice ridge is heterogeneous by ice volume content. What is the nature of this heterogeneity? This work is dedicated to the investigation of this issue.

Various methods of drilling are widely used for studying the ice ridges – mechanical drilling with motor-driven auger, electromechanical drilling, electric thermal drilling and hot water thermal drilling. In our work electric thermal drilling and hot water thermal drilling with penetration rate recording on a computer were used for this purpose.

The ice ridge geometry and internal structure are identified by means of processing of the thermodrilling records. This procedure is well known and described in many previous papers,

for example (Morev and Kharitonov, 2001; Kharitonov, 2005), etc. This technology is protected by patent of Russia No. 2153070, 2000 (Morev et al., 2000). The drilling rate depends on the power supply, ice porosity and ice temperature. The location of voids, hard and porous ice along the drilling hole is identified by the thermodrill penetration rate. The obligatory condition for this identification to be valid is drilling at constant thermal capacity or recording the changes of capacity during drilling. Within the segments of porous ice and, especially, the voids filled by snow, shuga or air, the penetration rate of thermodrill sharply increases. In addition, the distance from snow (ice) surface to the sea level is measured. The thermodrilling data processing gives such characteristics as the above-water and under-water parts of the ice cover, the boundaries of the consolidated layer (CL) of the ice ridge, the boundaries of the voids and the zones of ice of various porosity. Fig. 1 shows a schematic illustration of a typical first-year ridge, and it provides the definition of terms used in the paper.

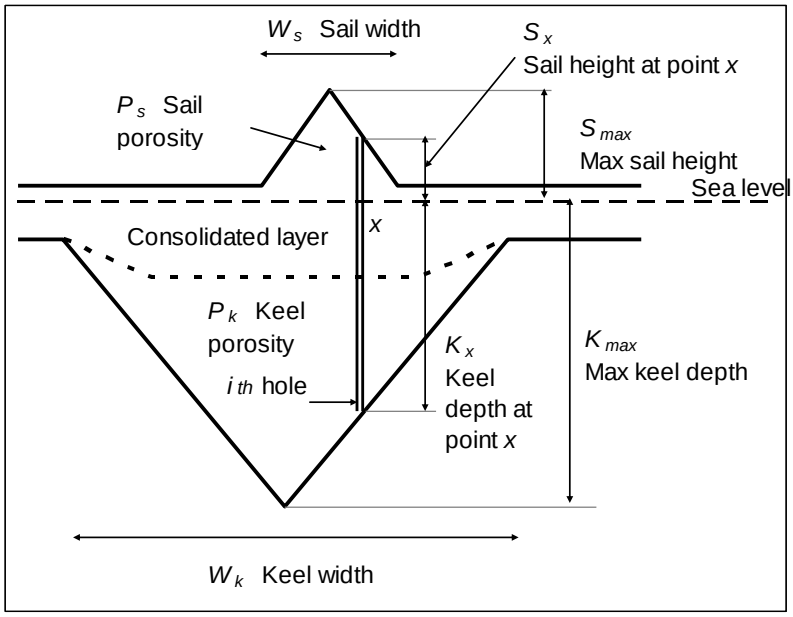

Figure 1. Schematic illustration of an ice ridge showing the definition of terms used in the paper.

METHODS

According to the energy conservation law, the relationship between the penetration rate V of the electric thermal drilling and the power supplied can be expressed by calorimetric formula (Kharitonov, 2008):

$$V = \frac{KP}{\Lambda\left(\rho(1-a-s)\left(-c_i t_i + L\right) - \rho_w s c_w t_i + \left(\rho(1-a-s) + \rho_w s\right) c_w t_w\right)}, \quad (1)$$

here P is the supplied power, K is the coefficient of heater efficiency which takes into account the heat dissipation through lateral surface of the heater, Λ is the area of middle-length section of the heater, ρ is the ice monocrystal density, a is the air volume content in ice, s is the brine volume content in ice, c_i is the heat capacity of pure ice, t_i is the ice temperature, L is the specific heat of ice melting, ρ_w is the melted water density, c_w is the heat capacity of melted

water, t_w is the temperature of melted water. We define the volumetric content of ice solid phase *VCI* as:

$$VCI = 1 - a - s. \quad (2)$$

I.e. *VCI* is 1 minus porosity. Value of *VCI* is similar to block coefficient but slightly less as it takes into account presence of pores in ice blocks.

Then from (1) and (2) the drill penetration rate *V* is inversely proportional to the volumetric content of the ice solid phase *VCI*:

$$VCI \approx \frac{K(VCI)P}{\Lambda\rho L} \cdot \frac{1}{V}, \quad (3)$$

where the expression *K*(*VCI*) indicates that technically the coefficient *K* may depend on the volumetric content of the solid phase of ice *VCI*. The nature of this dependence is unknown and hard to define. However, due to the high thermal inertia of the heater of the electric thermal drill and high penetration rate of hot water thermal drilling the influence of the volume content of ice solid phase *VCI* on the efficiency of the heater, i.e. on *K* factor, is offset. Thus, in first approximation we can assume that the coefficient of proportionality between the drill penetration inverse rate and the volumetric content of ice solid phase *VCI* in (3) does not depend on the magnitude of the volumetric content itself.

Fig. 2 as an example illustrates the dependence of the penetration inverse rate with the depth of borehole in the ice ridge.

In other words, it is the distribution of the volumetric content of the solid phase of ice along the borehole in relative terms, since the coefficient of proportionality has the dimension of penetration rate. Exact values of *VCI* are unknown as the coefficient of proportionality between *VCI* and 1/*V* is unknown. Therefore the values of 1/*V* as some relative units are used below for the values of *VCI* for simplification. Every borehole has its own specific distribution. Having averaged these distributions for all the holes, it is possible to obtain the average distribution of the volumetric content of the solid phase versus depth for the selected individual ice ridge or for the area investigated. Averaging is realized using the following procedure. All the depths h are considered in sequence from maximum value of ridge sail height S_{max} to maximum value of ridge keel depth K_{max} (see Fig. 1). 1/*V* values are averaged at each selected depth in all the boreholes corresponding to this depth. In the case, when this selected depth *h* exceeds ridge sail height or ridge keel depth in some borehole, two variants are possible. We can either exclude this borehole from averaging, or guess that the volumetric content of the ice solid phase in this point equals zero. Fig. 3 shows schematic illustration of second variant of averaging.

In the first case (Figure 4, line 1), number of distributions used for this averaging is various at different depths. The greater is this number, the more statistically correct is the volumetric content of the ice solid phase. However, the CL boundaries determined by this distribution are not valid, as the number of the distributions used for averaging is various at different depths, as it was mentioned above. Fig. 5 shows schematic illustration why this distribution is not suitable for determining the CL boundaries.

The second variant of averaging is as follows. At those boreholes *x* where the depth *h* under consideration goes beyond the limits of sail S_x or keel K_x, a value of 1/*V* is taken as zero. Fig. 4 (lines 2) shows examples of the results of such averaging for real thermal drilling data.

Limits of X-axis scale depend on the limits of changing of *V*. Let us examine this variant of averaging more thoroughly.

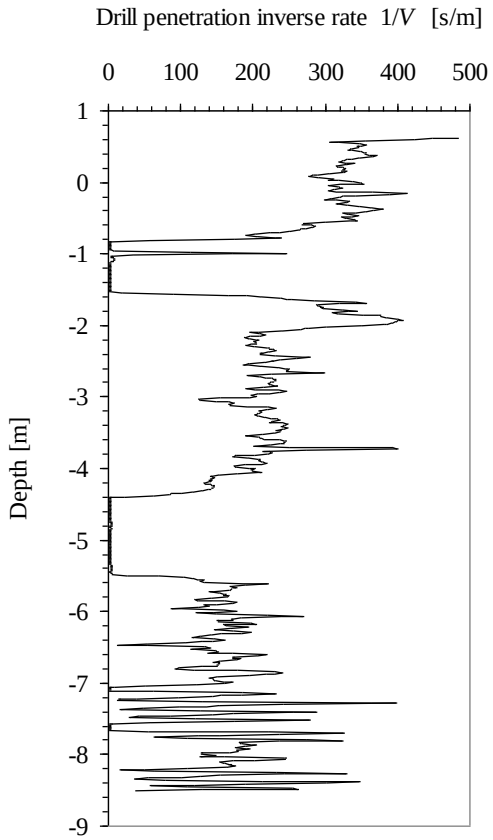

Figure 2. The dependence of the drill penetration inverse rate with the depth of drilling a borehole in the ice ridge.

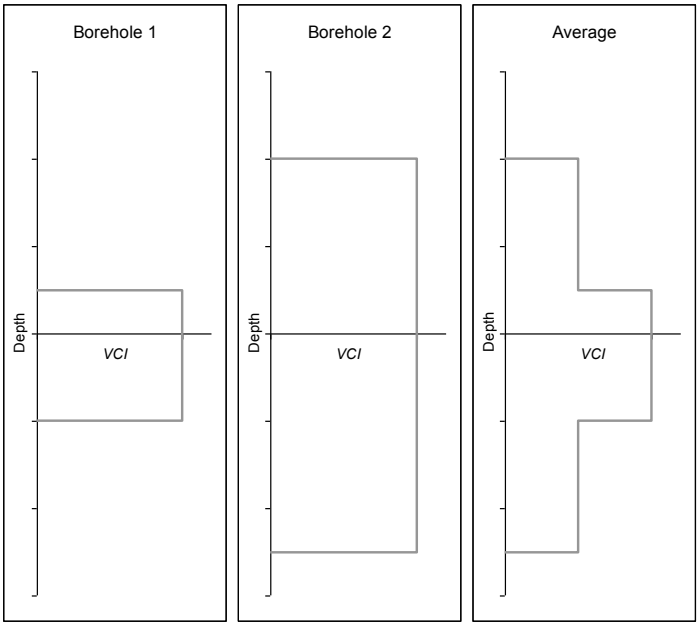

Figure 3. Schematic illustration of averaging of two depth-wise distributions of the volume content of ice solid phase (*VCI*).

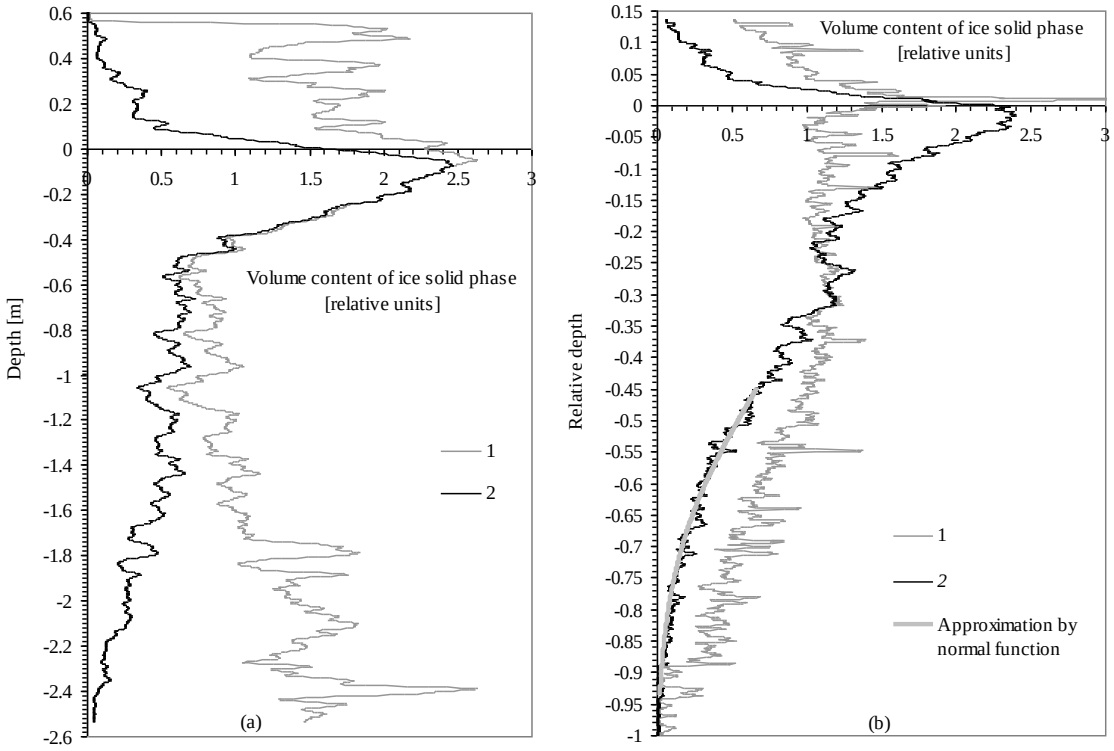

1 – when the number of averaged distributions is various at different depths; 2 – when the number of averaged distributions is equal at different depths.

Figure 4. Depth-wise distributions of the volume content of ice solid phase (*VCI*) of the two "mean statistical" ice ridges of different research areas (according to electric thermal drilling data).

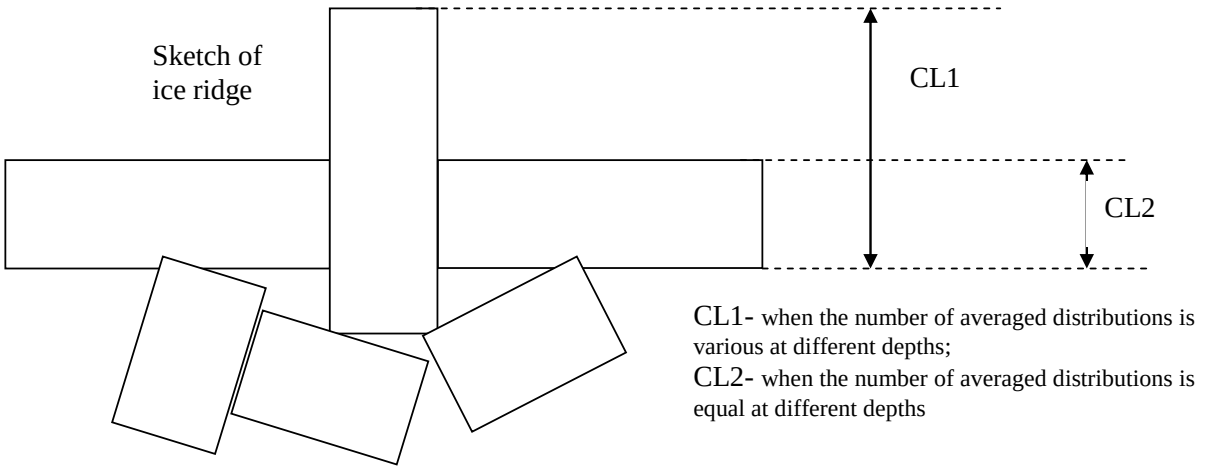

Figure 5. Schematic illustration is why distribution is not suitable for determining the CL boundaries when the number of averaged distributions is various at different depths.

SIMULATION

Let us imagine an ice ridge of ideal form, the sail and keel of which have a triangular shape, as shown in Fig. 1, and blocks of ice have zero micro porosity. How does the distribution of

the volume content of the solid phase of ice at depth look like for such an ice ridge, if we average a large number of individual distributions in the boreholes, evenly distributed across the width of the ice ridge W_k? Notably, in an ideal ice ridge the individual depth-wise distribution of the volume content of the ice solid phase at each point x will have the form of a step curve, where zero corresponds to voids, and one corresponds to ice. Averaging was executed the same way as shown in Fig. 3. This averaged distribution is shown in Fig. 6. The height of the ice ridge sail is randomly chosen to be 4 m, draft keel is 15 m. The entire graph can be divided into four areas determining the shape of the *VCI* curve (lines 1 in Fig. 6). The first area indicated in Fig. 6 as I, corresponds to the sail of the ice ridge. Area II corresponds to the above-water part of the CL. Area III corresponds to the underwater part of the CL. Area IV corresponds to the unconsolidated part of the keel of the ice ridge. Let us examine more thoroughly the shape of the *VCI* curve in each of these areas. Due to the fact that the shape of the ice ridge sail is chosen to be triangular, *VCI* graph in the sail area will be a straight line. The angle of inclination and the value of the 0-A interval intercepted by this line (line 2 in Fig. 6) on the X-axis, will be determined by W_s/W_k ratio, subject to zero porosity of sail P_s. In case $P_s \neq 0$

$$A = \frac{W_s}{W_k} \cdot (1 - P_s) \quad . \tag{4}$$

$$\mathrm{B} = (1 - P_k) \, . \tag{5}$$

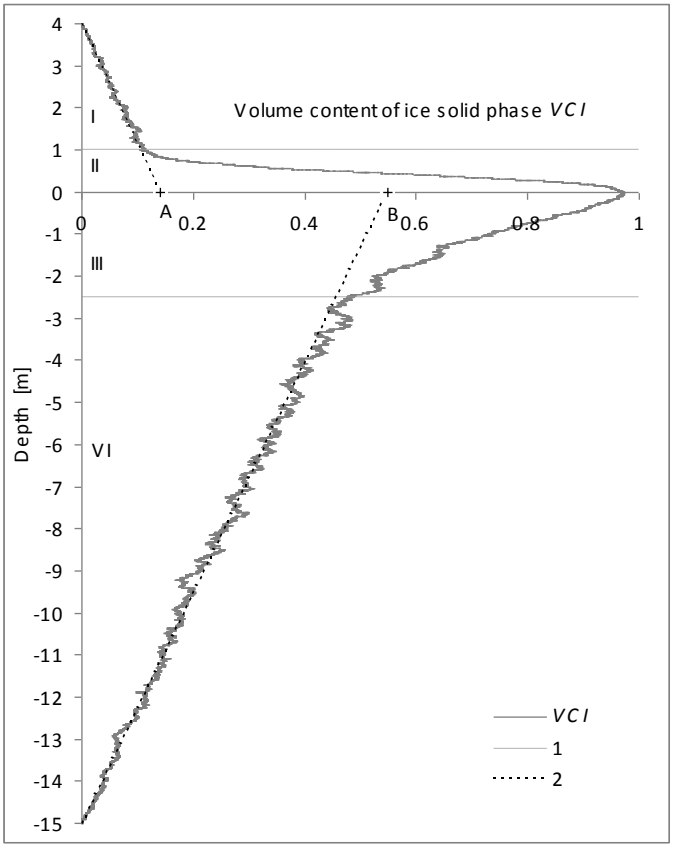

1 – Lines dividing the graph into various areas, 2 – lines intercepting 0-A and 0-B sections on the X-axis (explanation in text)

Figure 6. Depth-wise distribution of volume content of ice solid phase (*VCI*) for the ideal ice ridge shown in Fig. 1 obtained through averaging 1,000 records of drill penetration rate evenly distributed across the width of the ice ridge W_k.

In Fig. 7 behavior of the *VCI* curve of the ice ridge sail is illustrated for various shapes of the sail: triangular sail, semicircular sail (for comparison) and the Laplace distribution-shaped sail.

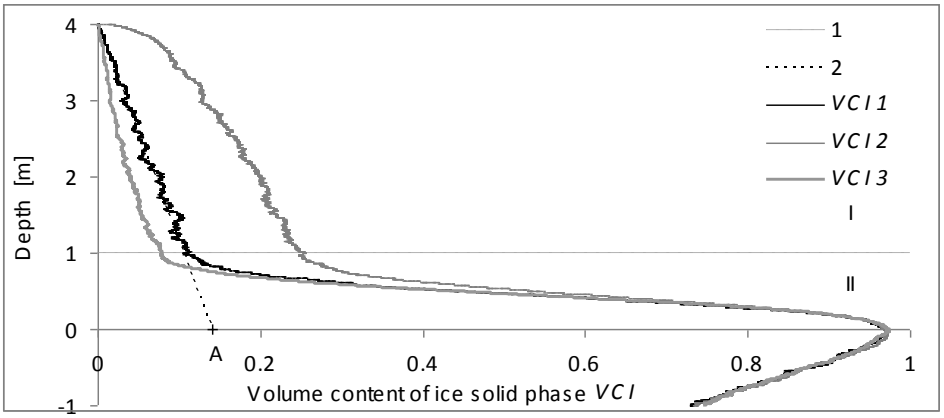

1 – Line dividing the graph into areas of sail and CL, 2 – line intercepting 0-A section on the X-axis (explanation in text); *VCI 1* – triangular sail; *VCI 2* – semicircular sail; *VCI 3* – Laplace distribution-shaped sail. All curves are plotted for single value of ice ridge sail porosity.

Figure 7. Depth-wise distribution of the volume content of ice solid phase (*VCI*) for an ice ridge sail of different shapes.

In the case the porosity of ice ridge sail depends on the depth, line 2 in Fig. 7, determining the course of *VCI*, is no longer a straight line, but will diverge towards *VCI* decrease. For example, increase of the porosity of the ice ridge sail with depth (to the negative direction along Y-axis) at triangular sail form will give the *VCI* divergence from the line 2, similar to the *VCI* 3 curve.

The behavior of the *VCI* curve in area II, corresponding to an above-water part of the CL will be determined by the law of distribution of the upper boundary of the CL. In fact, the *VCI* curve in area II is an integral probability distribution of the ice presence within this depth range, which is determined by the spread of the upper boundary of the CL. The same is for area III, corresponding to the underwater part of the CL. Fig. 8 shows examples of the *VCI* behavior for normal distribution of the upper and lower boundaries of the CL and for uniform distribution. Variances of location distributions of upper and lower boundaries of the CL are different, the higher the variance, the flatter is *VCI* variation with depth. With a uniform distribution of the position of the upper and lower boundaries of the CL, inclination angles of *VCI* curve in areas II and III are determined by range of variation of the position. For example, *VCI* 2 line in Fig. 8 shows that the upper boundary of the CL is uniformly distributed in the depth range of 0.22...0.64 m, and the lower boundary - in the depth range of -0.09...-1.88 m. Accordingly, due to significantly greater range of variation of the CL lower boundary, the *VCI* 2 line in area III is flatter than in area II. *VCI* 1 graph reaches the maximum value of 0.97. This suggests that the CL was absent in (1-0.97)·100 = 3 % of all boreholes.

Fig. 9 shows the behavior of the *VCI* curve for ice ridge keel of triangular shape under different conditions. *VCI* 1 represents a situation where the keel porosity is constant. *VCI* will have the same form as *VCI* 2, when the keel porosity is constant; however boreholes are evenly distributed not across the whole keel width W_k, but in a narrower range (in this example in the section where keel exceeds 8 m). *VCI* 3 shows a situation similar to *VCI* 2,

however the porosity of the ice ridge keel uniformly increases with depth (in the negative direction along Y-axis).

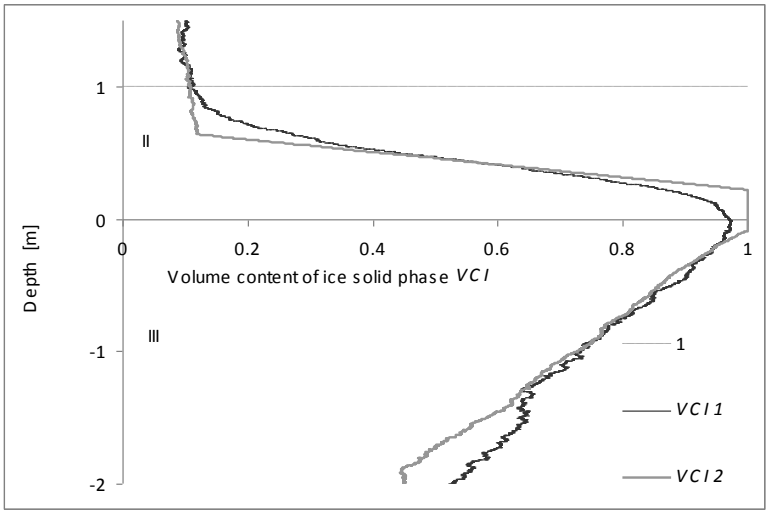

1 – Line dividing the graph into areas of sail and CL; *VCI 1* – normal distribution of the upper and lower boundaries of the CL; *VCI 2* – uniform distribution.

Figure 8. Depth-wise distribution of the volume content of ice solid phase (*VCI*) for CL of the ice ridge.

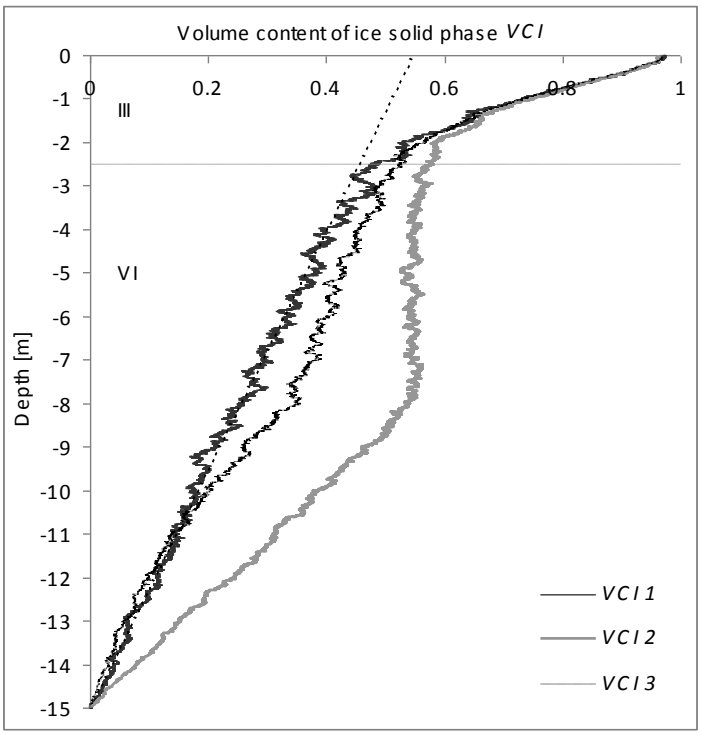

VCI 1 – keel porosity is constant; *VCI 2* – keel porosity is constant, however boreholes are evenly distributed not across the whole keel width W_k, but in a narrower range (in this example in the section where keel exceeds 8 m); *VCI 3* – similar to *VCI 2*, but the porosity of ice ridge keel uniformly increases with depth (in the negative direction along Y-axis).

Figure 9. Depth-wise distribution of the volume content of ice solid phase (*VCI*) for triangular-shaped keel of the ice ridge.

DISCUSSION

Of course, in real life it is not practicable to drill as many boreholes as used in the numerical experiment. Fig. 4(a) shows an example of depth-wise distribution of the volume content of the solid phase of ice *VCI* for an ice ridge of the Sea of Azov, investigated in 2005. This distribution was plotted based on 35 boreholes drilled evenly along two intersecting lines, perpendicular to the crest of the ice ridge. This example is indicative of the fact that the *VCI* in the range of depths (0.13...-0.47 m), corresponding to the CL has the shape of almost perfect triangle (line 2). This suggests that the upper and lower boundaries of the CL of the ice ridge are uniformly distributed. On this basis, we can easily estimate the average thickness of the CL.

Typically, during limited time of the expedition several ice ridges are investigated, and the number of boreholes drilled on each ice ridge can range from several to two or three dozens. Averaging the individual distribution of *VCI* for all boreholes, one can obtain generalized information, an average ice ridge for the area of research. The example of such distribution constructed by averaging 88 records of drill penetration rate for 14 ice ridges is shown in Fig. 4(b). Due to the fact that the *VCI* distributions of all ice ridges with different sail height, keel draft and porosity are averaged, the *VCI* curve is most informative with respect to CL boundaries and its average thickness (line 2). Within the depth range of -0.45...-1 *VCI* is well approximated by a normal Gaussian distribution function. In fact, this behavior of the *VCI* curve at the bottom part of the keel is determined by central limit theorem.

In May 2010, at Baidaratskaya Bay ice ridges were investigated using hot water drilling method with computer recording of the penetration rate. As an example Fig. 10 shows two unusual distributions of *VCI*, obtained by averaging 36 (ice ridge 17) and 21 (ice ridge 10) records of the penetration rate of drilling. As the penetration rate of hot water drilling is higher then the same of electric thermal drilling the X-axis scale differs from scale in Fig. 4.

Uncharacteristic behavior of *VCI* of the ice ridge 17 (Fig. 10a) in the CL area is that the upper boundary of the CL has become blurred. As it can be seen from the graph, the upper boundary of the CL changes within the depth range of 0.4...-1.4 m. Moreover, in the range of 0.4...0.25 m *VCI* curve behavior is similar to the ideal *VCI* 1 curve in Fig. 8. However, as the depth increases to -0.2 (in the negative direction of Y-axis) *VCI* doesn't increase. Only after this depth *VCI* begins to increase almost uniformly. In the depth area from -1.8 to -2.6, corresponding to the distribution of the lower boundary of the CL, *VCI* behavior corresponds to an ideal ice ridge. This distribution of *VCI* corresponding to the upper boundary of the CL is determined by the fact that the ice ridge was studied on June 2, when the upper layer of the CL was destructed by solar radiation. Part of the CL was screened by sail of ice ridge. On the graph this corresponds to the "step" of *VCI* with values 0.1...0.24.

In Fig. 10b *VCI* of the ice ridge 10 also has an unusual appearance, namely, the CL of the ice ridge is divided by thickness in two parts. This type of graph indicates that the ice ridge 10 is the result of secondary ridging. Already formed ice ridge is compressed, and as the result, ridging of the ice surrounding ice ridge happens. Thus, in the future the newly formed fragment of the resulting ice ridge will have the CL significantly thinner than the CL of fragment of old ice ridge.

When the number of boreholes drilled in the ice ridge increases, the ratio of the area under the *VCI* curve above the water level to the area under the *VCI* curve below the water level will asymptotically approach the value of the relative density difference of ice and water according to the condition of hydrostatic balance. Mathematically, it looks like this:

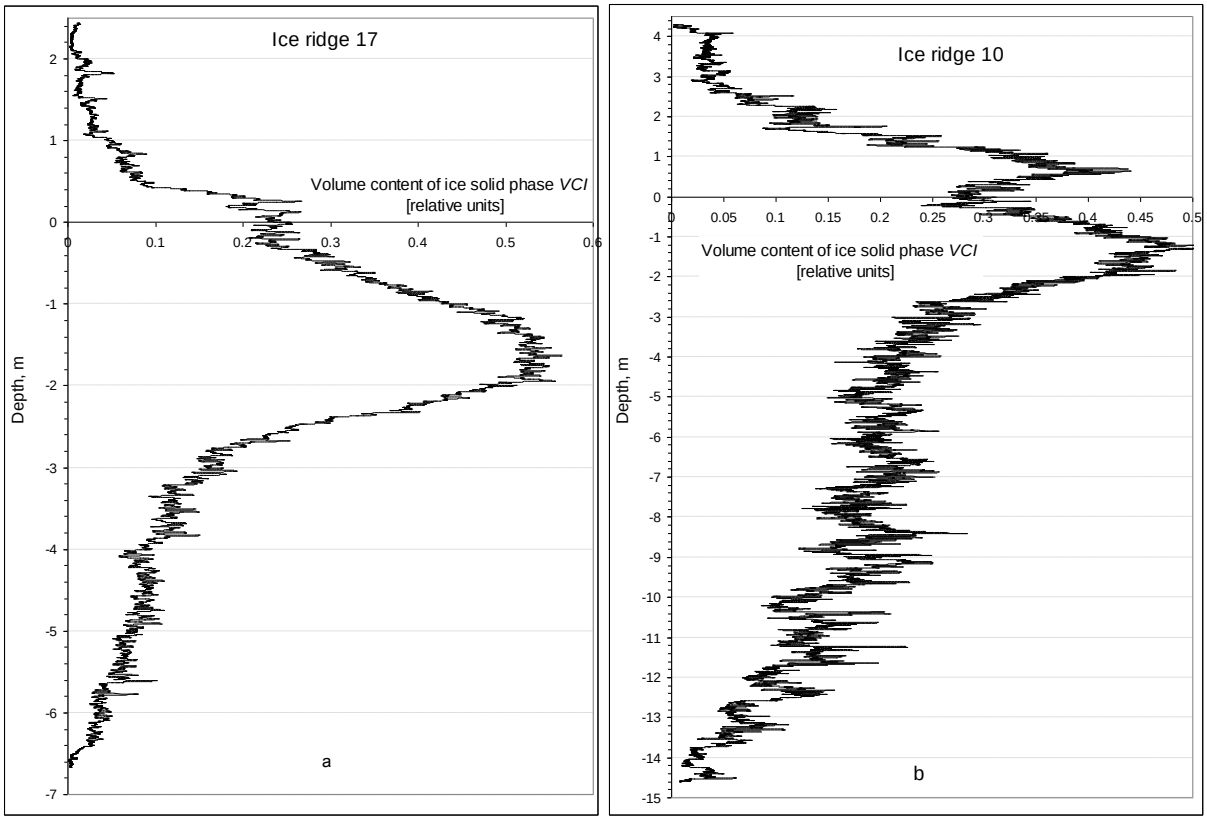

As the penetration rate of hot water drilling is higher then the same of electric thermal drilling the X-axis scale differs from scale in Fig. 4.

Figure 10. Depth-wise distribution of the volume content of ice solid phase (*VCI*) of two ice ridges investigated in 2010 in Baidaratskaya Bay (according to the hot water drilling data).

$$\frac{\int_0^{S_{max}} VCI \cdot dh}{\int_0^{K_{max}} VCI \cdot dh} \xrightarrow[n\to\infty]{} \frac{\rho_w - \rho_i}{\rho_i}, \quad (5)$$

where h is the depth, n is the number of boreholes in the ice ridge, ρ_i is the ice monocrystal density. In fact, the left-hand fraction in (5) is the ratio of ice masses of sail and keel. Thus, knowing the density of water in the area of research, using the right part of formula (5) the ideal ratio of ice masses of sail and keel can be calculated. By comparing how the real balance of sail and keel ice masses differs from the ideal, it is possible to conclude whether the studied ice ridge is in a state of hydrostatic equilibrium. It should be borne in mind that the sail and keel mass ratio is influenced by the mass of snow located on the ice ridge.

CONCLUSION

Distribution of *VCI* provides information about the consolidated layer of ice ridge. By type of *VCI* curve, the laws of boundaries distribution of the CL of ice ridge (or a group of ice ridges) and the average thickness of the CL can be estimated. There is an opportunity to see the changes in structure of the CL and estimate its uniformity.

REFERENCES

Kharitonov, V.V., 2005. Peculiarities of Fractional Composition of the Pechora Sea First-Year Ridges. Proc. of the 18th Int. Conference on Port and Ocean Engineering under Arctic Conditions (POAC). Potsdam, New York, V. 2, pp. 907-916.

Kharitonov, V.V., 2008. Internal structure of ice ridges and stamukhas based on thermal drilling data. Cold Regions Science and Technology. 52/3 pp. 302-325.

Morev, V., Kharitonov, V., 2001. Definition of the Internal Structure of Large Ice Features by Thermal Drilling Methods. Proc. of the 16th Int. Conf. on Port and Ocean Engineering under Arctic Condition. POAC`01. Aug. 12-17, 2001 Ottawa, Ontario, Canada. Vol.3, p.1465-1472.

Morev.V.A., Morev A.V., Kharitonov V.V., 2000. Method of determination of ice ridge and stamukha structure, ice features and boundaries of ice and ground. License of Russia № 2153070, Bulletin of inventions № 20 (in Russian).